

CONTACT SOLUTION ALGORITHMS

John T. Tielking  
Texas A and M University  
College Station, Texas

EXPANDED ABSTRACT

Two algorithms for obtaining static contact solutions are described in this presentation. Although they were derived for contact problems involving specific structures (a tire and a solid rubber cylinder), they are sufficiently general to be applied to other shell-of-revolution and solid-body contact problems.

The shell-of-revolution contact algorithm is a method of obtaining a point load influence coefficient matrix for the portion of shell surface that is expected to carry a contact load. If the shell is sufficiently linear with respect to contact loading, a single influence coefficient matrix can be used to obtain a good approximation of the contact pressure distribution. Otherwise, the matrix will be updated to reflect nonlinear load-deflection behavior.

The solid-body contact algorithm utilizes a Lagrange multiplier to include the contact constraint in a potential energy functional. The solution is found by applying the principle of minimum potential energy. The Lagrange multiplier is identified as the contact load resultant for a specific deflection.

At present, only frictionless contact solutions have been obtained with these algorithms. A sliding tread element has been developed to calculate friction shear force in the contact region of the rolling shell-of-revolution tire model. This element allows a relatively general, non-Coulomb, friction law to be specified for the contact interface. It has the added advantage of allowing friction to be calculated in the continuous interface and, when coupled with the solid-body contact algorithm, will permit analytic investigation of various continuum friction theories that have been proposed.

The outline of future directions for the development of contact solution algorithms is:

- I. SHELL-OF-REVOLUTION CONTACT ALGORITHM
- II. SOLID-BODY CONTACT ALGORITHM
- III. STATIC AND ROLLING CONTACT FRICTION
- IV. FUTURE DIRECTIONS FOR CONTACT SOLUTION ALGORITHMS

PRECEDING PAGE BLANK NOT FILMED

## I. SHELL-OF-REVOLUTION CONTACT ALGORITHM

A shell whose geometry and material properties are axisymmetric can be economically modeled by shell-of-revolution finite elements. The SAMMSOR/SNASOR programs (refs. 1,2), for example, permit nonlinear behavior of orthotropic shells of revolution to be calculated, including response to nonaxisymmetric loads. The algorithm described here was developed to calculate the shell deflection in response to a nodal point load, utilizing the calculated response to a sequence of harmonically varying ring loads on the node. The point load solution is then used to construct an influence coefficient matrix, from which the shell contact solution is obtained.

## FINITE-ELEMENT TIRE MODEL

The tire is modeled here by an assembly of axisymmetric shell elements connected to form a meridian of arbitrary curvature and following the carcass mid-surface. The elements are homogeneous orthotropic, with moduli determined by the ply structure of a particular tire. Details of this model are given in reference 3. If the deformation is symmetric about the wheel plane only one-half of the meridian is modeled, as shown in figure 1. The finite elements are joined at nodal circles, referred to here as nodes. Node 12 in figure 1 is located at the tire bead and is given in built-in end condition.

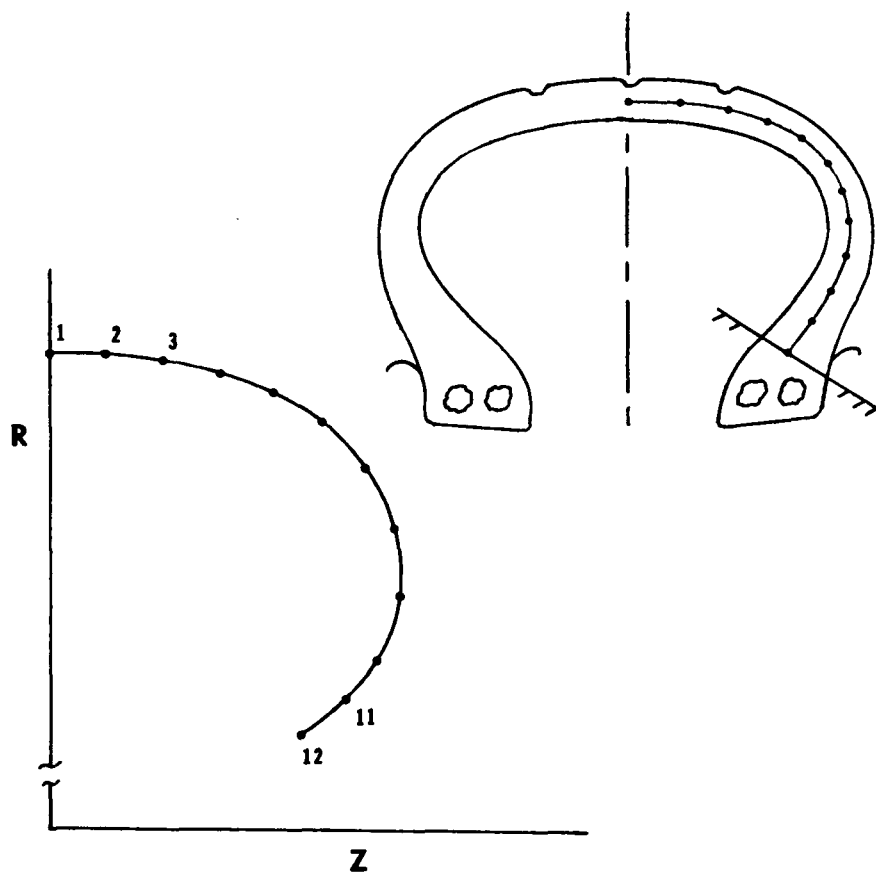
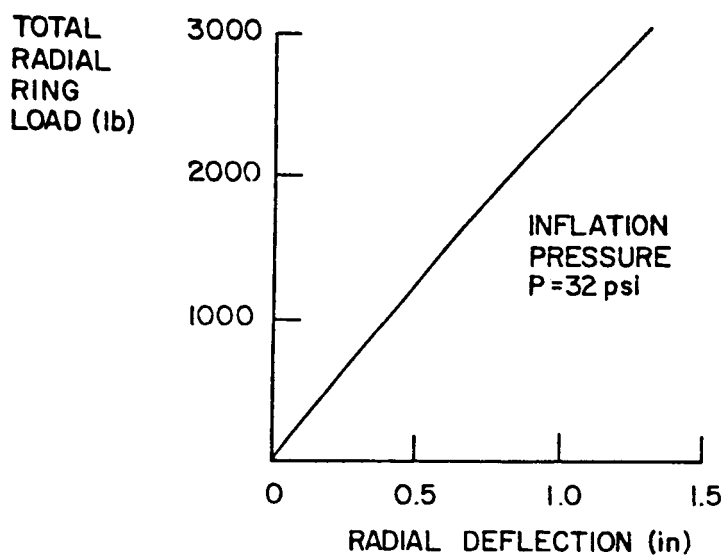


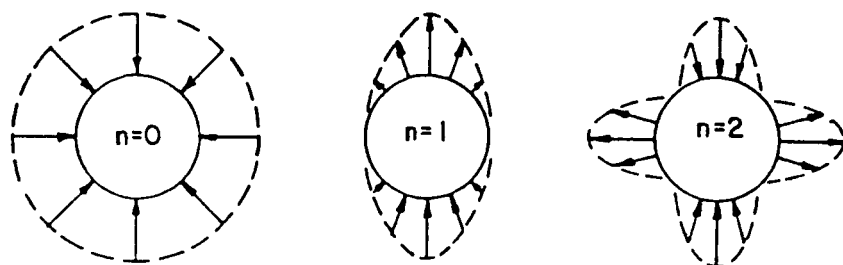
Figure 1

## SINGLE HARMONIC RING LOADS

The finite-element tire model will respond to single harmonic ring loads on the nodal circles in addition to a uniform inflation pressure load. An approximately linear ring load-deflection response is obtained when an individual ring load is applied to any node of the pressurized tire model. An example ring load-deflection calculation for a passenger tire model is shown in figure 2. A harmonic sequence of stiffness matrices is obtained by applying a sequence of single harmonic ring loads to each of the nodes that may be in the tire-pavement contact region.



CROWN LOAD-DEFLECTION DATA CALCULATED WITH A UNIFORM RING LOAD APPLIED TO THE CROWN NODE



SINGLE HARMONIC RING LOADS APPLIED TO A FINITE-ELEMENT NODE

Figure 2

### TRANSFER FUNCTION DEFINITION

As a consequence of the linearity of the ring load-deflection response, the application of a single harmonic ring load produces a displacement field that varies circumferentially in the same harmonic as the applied ring load. The definition of the transfer function  $T_n$  as the ratio of the output and input amplitudes is given below (ref. 4). Since each node responds differently, a transfer function matrix  $T_{ik|n}$  is used to store the stiffness information generated by the ring loads. The partitions of this matrix are determined by the direction of the ring load. (Fig. 3).

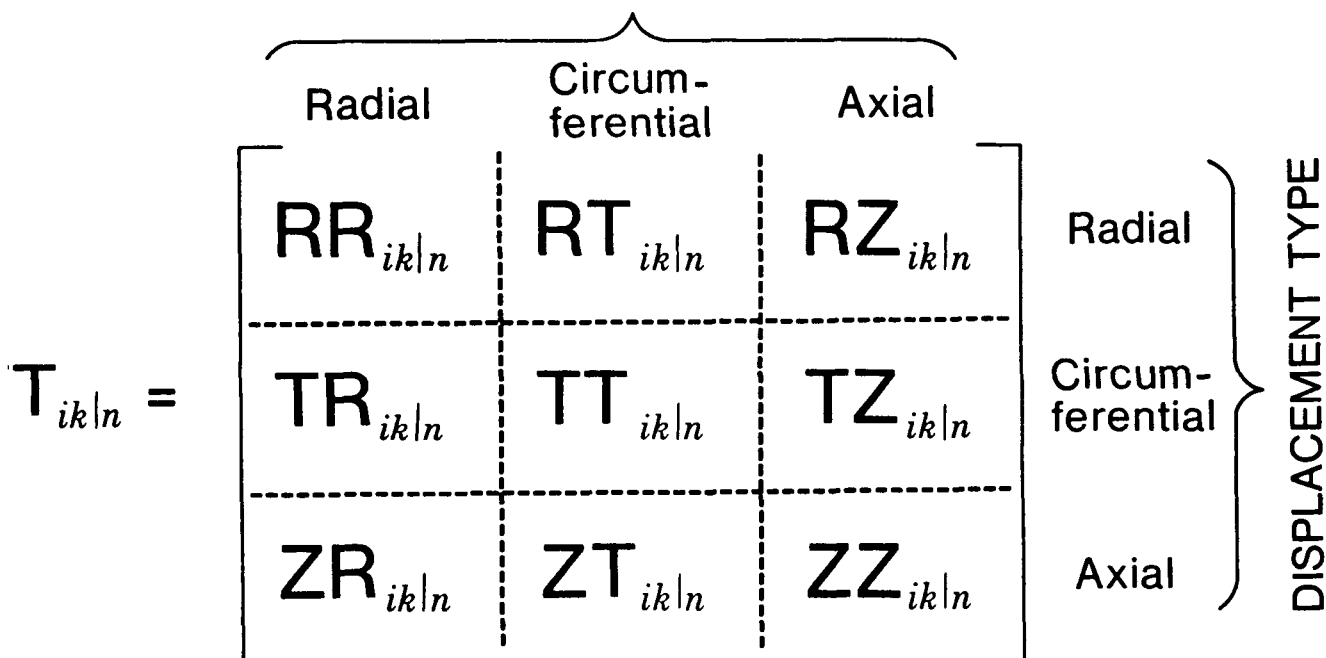
Single Harmonic Ring Load       $A_n \cos n\theta$  (input)

Single Harmonic Displacement       $B_n \cos n\theta$  (output)

$$\text{TRANSFER FUNCTION } T_n = \frac{B_n}{A_n}$$

$T_{ik|n}$  =  $n^{\text{th}}$  harmonic transfer function relating displacement of node i to an  $n^{\text{th}}$  harmonic ring load on node k

### LOAD TYPE



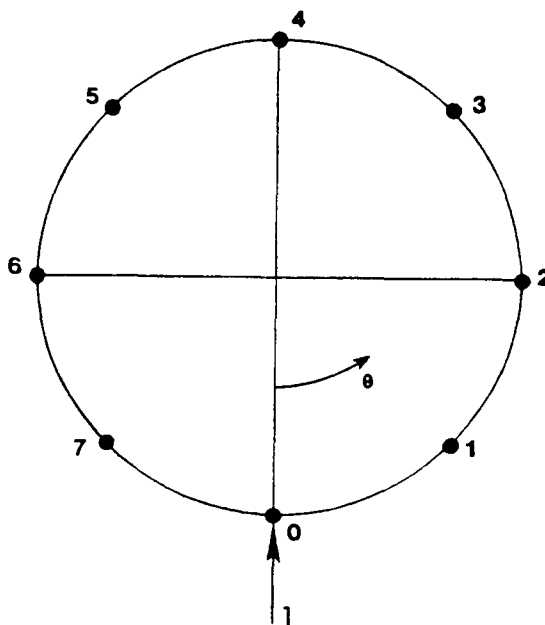
$$n=0,1,\dots,N/2$$

Figure 3

## POINT LOAD VECTOR $\{p\}$ AND THE DISCRETE FOURIER TRANSFORM (DFT)

This application of the discrete Fourier transform uses an even number of points ( $N$ ), equally spaced around the circumference. The example shown in figure 4 uses  $N=8$  points. A unit load is applied at any point, say point 0. The DFT of the load vector yields a set of  $N$  coefficients,  $G_j$ , which are approximate values of the coefficients of the conventional Fourier series defined on the continuous interval  $0 \leq \theta \leq 2\pi$  and representing the unit point load. The point load is applied, sequentially, in the radial, axial, and circumferential directions.

### INFLUENCE COEFFICIENT GENERATION



$$\{p\} = \{1, 0, 0, 0, 0, 0, 0, 0\} \quad \text{load vector}$$

$$\text{DFT } G_j = \frac{1}{N} \sum_{k=0}^{N-1} g_k w_e^{jk} \quad w_e = e^{-i2\pi/N}$$

$$g_k = \{p\}, \quad G_j = \frac{1}{N} \quad j = 0, 1, \dots, N-1$$

Figure 4

## INVERSE DISCRETE FOURIER TRANSFORM (IDFT) AND THE INFLUENCE COEFFICIENTS

Having the unit point load represented by a conventional Fourier series, whose coefficients  $a_n$  are approximately given by the DFT coefficients, the transfer functions  $T_{ik|n}$  are applied, on each harmonic, to obtain the coefficients  $b_n$  of the Fourier series representing the response of the nodal circle to the unit point load. The inverse discrete Fourier transform is then used to evaluate the displacements,  $u_m$ , at the N points. These displacements are the elements of the influence coefficient matrix  $[A_{ijkl}]$ . (Fig. 5).

$$\text{INPUT SERIES COEFFICIENTS } a_n \approx G_n = \frac{1}{N}$$

$$\text{OUTPUT SERIES COEFFICIENTS } b_n = a_n T_{ik|n} = \frac{1}{N} T_{ik|n}$$

$$\text{DFT OF DISPLACEMENT VECTOR } G_n \approx b_n$$

$$\text{IDFT } u_m^{ik} = \sum_{n=0}^{N-1} G_n W_e^{-mn} \quad m = 0, 1, \dots, N-1$$

$$\text{INFLUENCE COEFFICIENTS } A_{ijkl} = u_{j-1}^{ik} \quad j = 1, 2, \dots, N$$

$$\text{SHIFT: } A_{ijk\ell} = u_{j-\ell}^{ik} \quad j = \ell, \ell+1, \dots, N$$

$$\text{SYMMETRY: } A_{klij} = A_{ijkl}$$

$$\{d_{ij}\} = [A_{ijkl}] \{P_{kl}\}$$

Figure 5

### INFLUENCE COEFFICIENT MATRIX

The influence coefficient matrix relates the radial, axial, and circumferential components of the displacement of points on the tire surface to the radial, axial, and circumferential components of load at these points. The radial response partition, shown in figure 6, is used to obtain a solution for frictionless contact, in which the axial and circumferential force components are known to be zero. The matrix here covers 3 points on each of 5 nodes. The point separation with this matrix is 11.25 degrees.

$$\begin{matrix}
 \left. \begin{matrix} d_{11} \\ d_{21} \\ d_{31} \\ d_{41} \\ d_{51} \\ d_{12} \\ d_{22} \\ d_{32} \\ d_{42} \\ d_{52} \end{matrix} \right\} & = & \left[ \begin{matrix} A_{1111} & & & & \\ A_{2111} & A_{2121} & & & \\ A_{3111} & A_{3121} & A_{3131} & & \\ A_{4111} & A_{4121} & A_{4131} & A_{4141} & \\ A_{5111} & A_{5121} & A_{5131} & A_{5141} & A_{5151} \\ A_{1211} & A_{1221} & A_{1231} & A_{1241} & A_{1251} & A_{1212} \\ A_{2211} & A_{2221} & A_{2231} & A_{2241} & A_{2251} & A_{2212} & A_{2222} \\ A_{3211} & A_{3221} & A_{3231} & A_{3241} & A_{3251} & A_{3212} & A_{3222} & A_{3232} \\ A_{4211} & A_{4221} & A_{4231} & A_{4241} & A_{4251} & A_{4212} & A_{4222} & A_{4232} & A_{4242} \\ A_{5211} & A_{5221} & A_{5231} & A_{5241} & A_{5251} & A_{5252} & A_{5222} & A_{5232} & A_{5242} & A_{5252} \end{matrix} \right] \left. \begin{matrix} \{d_{ij}\} = [A_{ijk}] \quad \{P_{kl}\} \\ P_{11} \\ P_{21} \\ P_{31} \\ P_{41} \\ P_{51} \\ P_{12} \\ P_{22} \\ P_{32} \\ P_{42} \\ P_{52} \end{matrix} \right\}
 \end{matrix}$$

Figure 6

### TOROIDAL SHELL CONTACT SCHEMATIC

A cylindrical coordinate system is used to locate points on the toroidal surface. The coordinates  $r$ ,  $\theta$ , and  $z$  indicate the radial, circumferential, and axial directions, respectively. The tire equator lies in the  $r-\theta$  plane (wheel plane) and a tire meridian is in an  $r-z$  plane.

After the inflation solution has been obtained, the tire model is deflected against a frictionless, flat surface. The contacting surface is perpendicular to the wheel plane and positioned at the specified loaded radius  $R_l$ , as shown in figure 7. The vertical load and the contact pressure distribution are unknown, *a priori*.

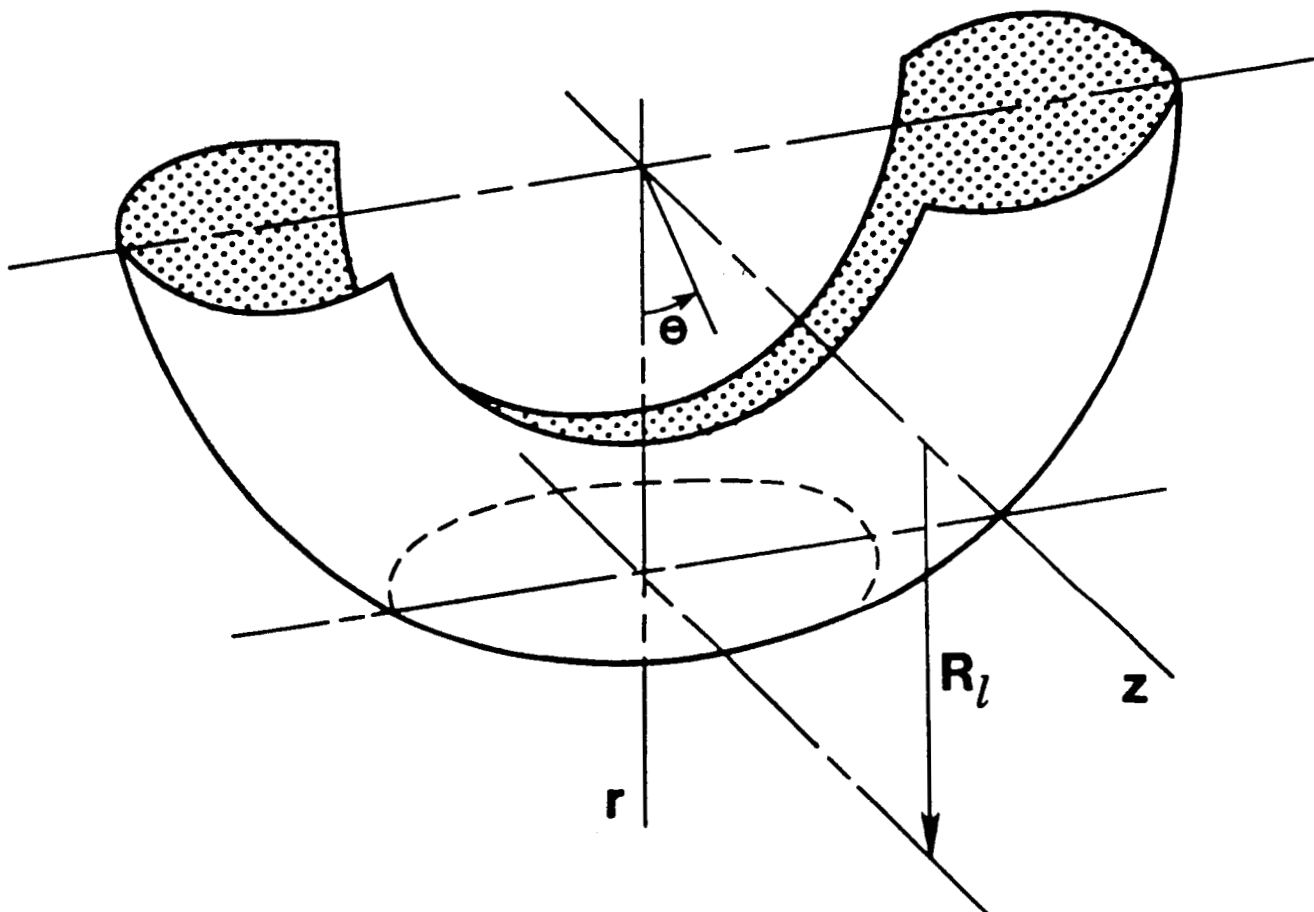


Figure 7

### DEFLECTED MERIDIAN

The deflected shape of the meridian passing through the center of contact is shown in figure 8. This shape is calculated by the finite-element tire model for the specified tire deflection of one inch. The tire load that will produce a one inch tire deflection is calculated to be 10,590 lb. Figure 8 also shows the meridian prior to inflation and the calculated shape of the meridian of the inflated tire, prior to contact loading. These finite-element meridians follow the carcass midsurface, as indicated in figure 1. Geometric and material property data on the Space Shuttle nose gear tire were used for the calculated results shown in figures 8, 9, and 10.

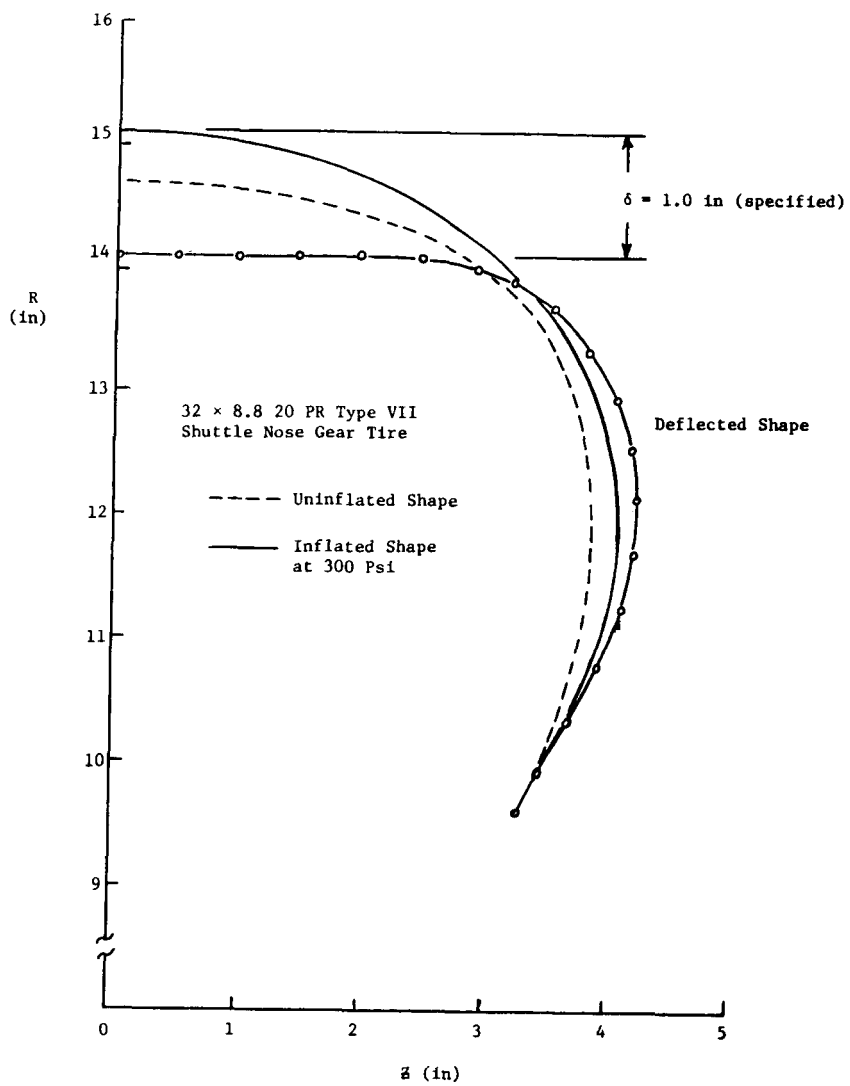


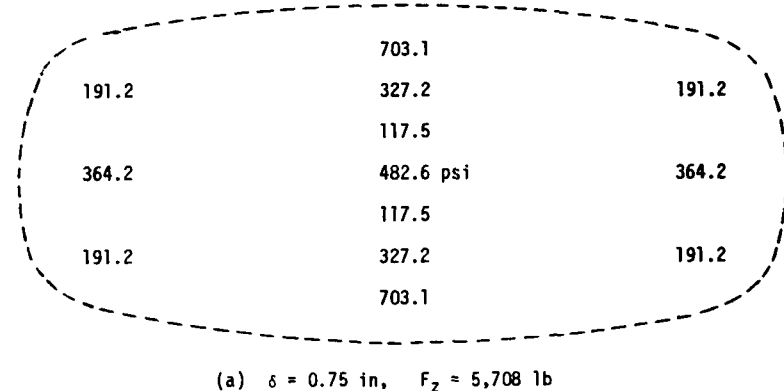
Figure 8

## CONTACT PRESSURE DISTRIBUTIONS

The static contact pressure values (psi) calculated for two different loads on the Shuttle nose gear tire are shown in figure 9. The number of finite-element points in the contact region increases as the tire load increases. A rough estimate of the contact boundary is obtained by extrapolation of the pressure distribution. Integration of the pressure distribution gives the tire load.

NOSE GEAR TIRE CONTACT PRESSURE DISTRIBUTIONS

32x8.8 20 PR TYPE VII  
Inflation Pressure = 300 psi



(a)  $\delta = 0.75$  in,  $F_z = 5,708$  lb

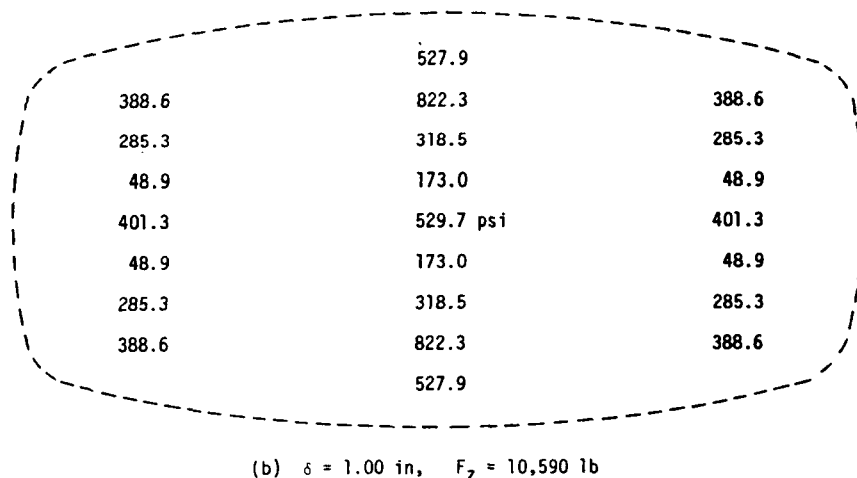


Figure 9

## TIRE LOAD VERSUS TIRE DEFLECTION

An important test of a tire model is its ability to calculate a static load-deflection curve. Figure 10 compares the load-deflection curve calculated for the Shuttle nose gear tire with measured data for a similar aircraft tire. Although these are both  $32 \times 8.8$  Type VII tires, constructional details can alter the load-deflection curve (and many other aspects of tire behavior). The cord used in the test tire is unknown and may be quite different from the nylon cord in the Space Shuttle tire.

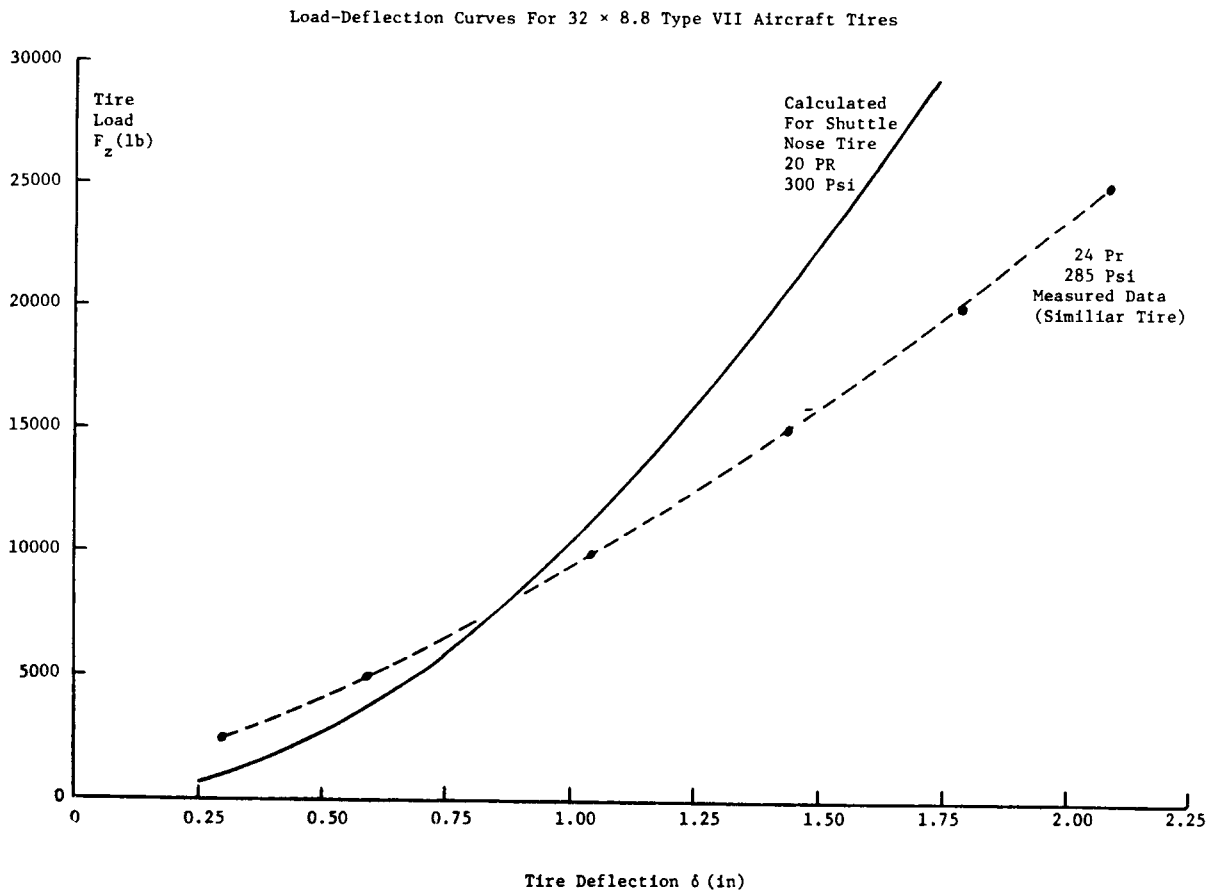


Figure 10

## II. SOLID-BODY CONTACT ALGORITHM

A solid body with a cylindrical surface is often loaded in contact against a rigid surface. The contact load may revolve around the body, as in the case of a roller or a solid tire, or may remain stationary if the cylinder is used as a support cushion.

Interfacial friction, present in all contact problems, is currently an active field of research. The study of frictional behavior is facilitated if the contact region is relatively large, as is produced when the body is highly deformable. This makes it easier to calculate distributions of normal pressure and tangential motion (slip) in the interface. In the case of rubber contact, the behavior deviates sufficiently from the Coulomb friction law that other, more physically realistic laws, can be easily tested. Since friction is a microscopic phenomenon, a contact solution giving continuous distributions of interfacial pressure and slip is desirable for analytic purposes. The contact algorithm described here provides a continuum solution for frictionless contact, the first step toward analysis of friction in the continuous contact interface.

### A PLANE STRAIN CONTACT PROBLEM

An elastic semicylinder of radius  $R$  is bonded to a fixed surface, figure 11(a). A contact load is applied by a rigid plate that deflects the semicylinder as shown in figure 11(b).

The problem is formulated in terms of cylindrical material coordinates  $(r, \theta, z)$  which identify points in the undeformed body,  $B_0$ . A point  $P_0$  in  $B_0$  is located by Cartesian coordinates  $x_1$  and  $x_2$  axes shown in figure 11(a) and

$$x_1 = r \cos \theta$$

$$x_2 = r \sin \theta$$

$$x_3 = z$$

The contact load is assumed to produce a plane strain deformation. Point  $P_0$  moves to position  $P$  in the deformed body,  $B$ . Point  $P$  is located by the Cartesian coordinates  $y_1$ . With plane strain,  $y_1 = y_1(r, \theta)$ ,  $y_2 = y_2(r, \theta)$ , and  $y_3 = \lambda_3 z$  where  $\lambda_3 = 1$  is a specified constant extension ratio.

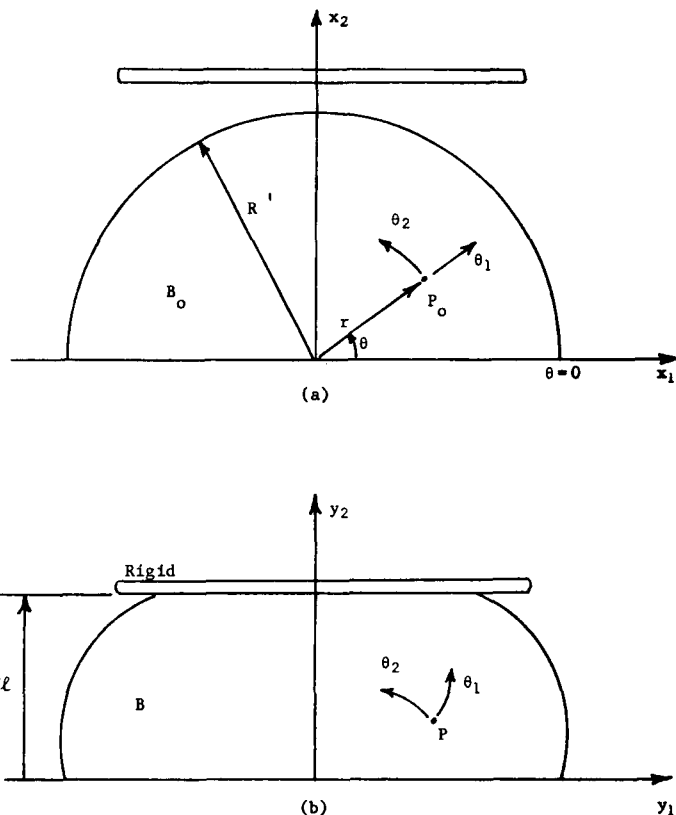


Figure 11

### GEOMETRIC DESCRIPTION

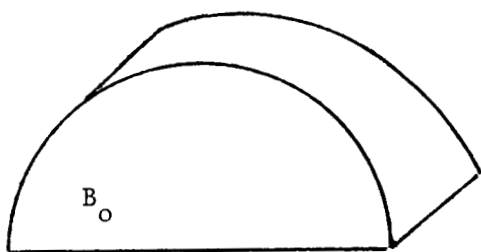
The metric tensors  $g_{ij}$  and  $G_{ij}$ , given below, completely describe the elastic semicylinder before and after deformation. Since  $y_3$  is known *a priori*, the problem is solved by finding the functions  $y_1(r, \theta)$  and  $y_2(r, \theta)$  which determine  $G_{ij}$ . The displacement field is not utilized in this formulation but it can, of course, be found when  $x_i$  and  $y_i$  are known. (Fig. 12).

$$g_{ij} = \begin{bmatrix} 1 & 0 & 0 \\ 0 & r^2 & 0 \\ 0 & 0 & 1 \end{bmatrix} \quad g^{ij} = \begin{bmatrix} 1 & 0 & 0 \\ 0 & r^{-2} & 0 \\ 0 & 0 & 1 \end{bmatrix}$$

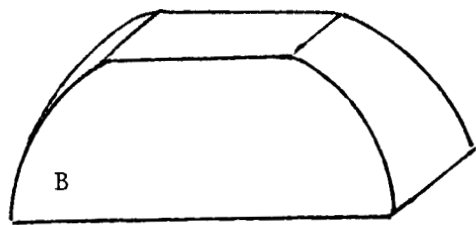
$$G_{ij} = \begin{bmatrix} y_{\alpha,1} & y_{\alpha,1} & 0 \\ y_{\alpha,2} & y_{\alpha,1} & 0 \\ 0 & 0 & \lambda_3^2 \end{bmatrix} \quad (\text{implied sum with } \alpha = 1, 2)$$

The Green/Saint-Venant strain tensor components are defined as

$$\gamma_{ij} = \frac{1}{2}(G_{ij} - g_{ij})$$



Undeformed  
Metric  $[g_{ij}]$



Deformed  
Metric  $[G_{ij}]$

Figure 12

## MATERIAL DESCRIPTION

The material is assumed to be hyperelastic so that its constitutive properties are contained in a strain energy density,  $W$ . Isotropy is also assumed. For plane strain of an isotropic material, the strain energy is known to be a function of only the first and third strain invariants,  $I_1$  and  $I_3$  (ref. 5)

$$W = W(I_1, I_3)$$

For general deformation, the strain invariants are given by

$$I_1 = g^{ij} G_{ij} \quad I_3 = G/g$$

where  $g = \det [g_{ij}] = r^2$  for the semicylinder and  $G = \det [G_{ij}]$ .

When the material is also assumed to be incompressible ( $I_3 = 1$ ) the constitutive behavior is not completely determined by the strain energy density. Hydrostatic pressure becomes an additional unknown, which can be determined as a Lagrange multiplier (ref. 6). This difficulty is avoided if a compressible material model is used.

The material description selected for the contact problem solved here is the compressible neo-Hookean model developed for continuum rubber by Blatz and Ko (ref. 7). The Blatz-Ko model may be expressed as

$$W(I_1, I_3) = \frac{1}{2}\mu(I_1 - 3I_3) + \frac{1}{k}K\left(\frac{\frac{1}{2}}{3} - \frac{k}{k-1} + \frac{\frac{1}{2}(1-k)}{k-1}\right)$$

where  $\mu$  is the classical shear modulus,  $K$  is the bulk modulus, and  $k$  is a parameter related to atomic repulsion. When  $I_3 = 1$ , the Blatz-Ko model reduces to the neo-Hookean model for incompressible material. For small strains it reduces to the energy density giving Hooke's law for compressible isotropic material.

## CONTACT CONSTRAINT

The assumption of frictionless contact with a rigid surface, positioned perpendicular to the  $y_2$  axis (see fig. 11(b)), implies a geometric constraint only on the solution function  $y_2(r, \theta)$ . Within the contact region, whose extent is not known *a priori*, the deformed surface is flat and it is known that  $y_2 = R_\ell$  where  $R_\ell$  is the specified location of the contact surface. Outside the contact region, and in the interior of  $B$ , the solution must satisfy  $y_2 < R_\ell$ . This inequality constraint on  $y_2$  is converted to an equality constraint by introducing a new function  $s(r, \theta)$ , defined by the following equation

$$y_2 + s^2 = R_\ell \quad (\text{constraint equation})$$

which is valid everywhere on the boundary and in the interior of  $B$ . The function  $s(r, \theta)$ , called a slack variable, has been used previously in optimization problems with an inequality constraint. Reference 8 gives several examples of the use of slack variables.

The contact problem is solved by minimizing the strain energy in  $B$ , subject to the constraint equation given above. Since plane strain is assumed, the energy is uniform along the axis of the semicylinder. Using symmetry, integration of the energy density is taken over one-half of the  $r-\theta$  plane contained in  $B_o$ .

The constraint equation is brought into the energy density functional by means of a Lagrange multiplier function  $\lambda(r, \theta)$ . The contact problem is then governed by the following functional

$$I(y_1, y_2, s, \lambda) = \iint F(r, \theta, y_1, y_2, s, \lambda) dr d\theta$$

where

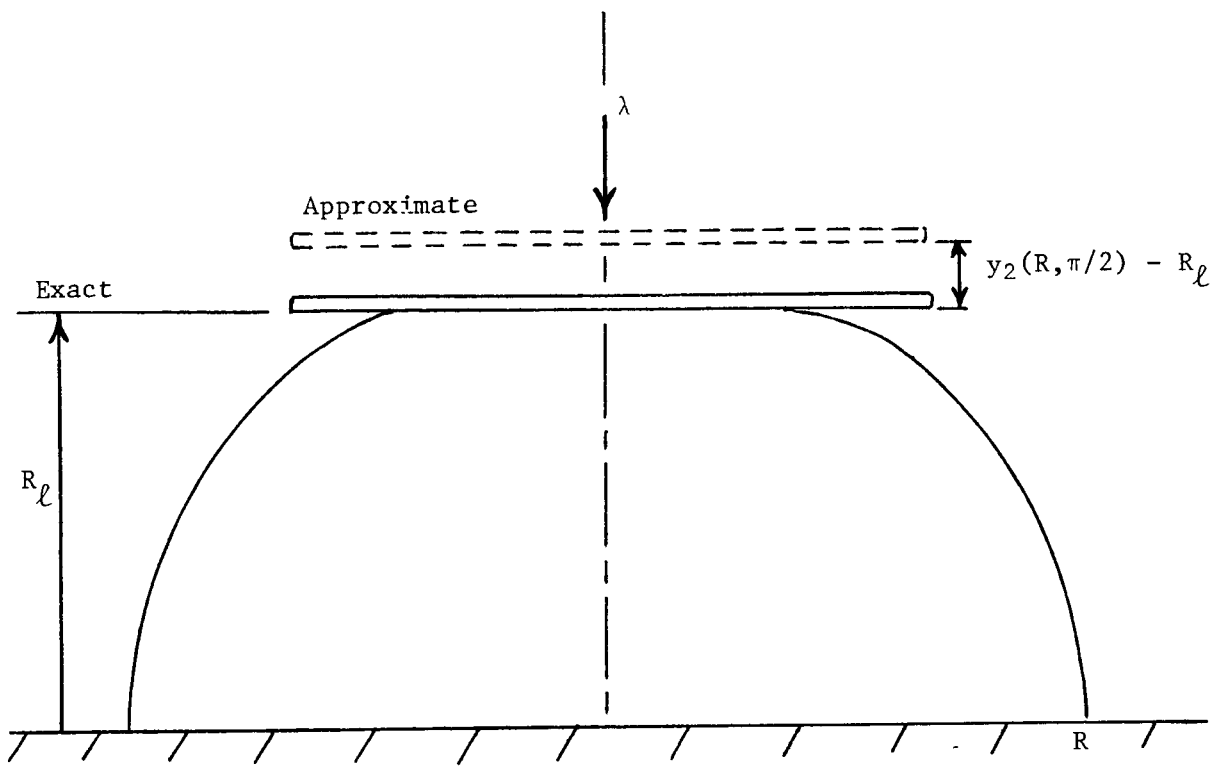
$$F = rW(y_{\alpha}, \beta) + \lambda (y_2 + s^2 - R_\ell)$$

Although  $rW$  is positive definite,  $F$  is not positive definite due to the addition of the constraint. Therefore,  $I$  may only be regarded as being made stationary instead of minimized by equilibrium solution functions. The integral of  $W$ , however, is minimized by the equilibrium solution and this is used as a check during the solution finding process.

Through additional analysis (J. T. Tielking, Texas A and M University, unpublished data) the Lagrange multiplier function is shown to be an unknown constant, identified as the resultant load in the contact region. The constraint condition may then be removed from the integral, the slack variable is no longer needed, and the contact problem is now governed by

$$I(y_\alpha, \lambda) = \iint rW(y_\alpha, \beta) dr d\theta + \lambda (y_2(R, \pi/2) - R_\ell)$$

The solution is obtained by finding  $y_\alpha(r, \theta)$  and the constant  $\lambda$  which make  $I(y_\alpha, \lambda)$  stationary. (Fig. 13).



Example:  $M = N = 2$

$$y_2(R, \pi/2) = R + (b_{11} - b_{12})R + (b_{21} - b_{22})R^2$$

Figure 13

## SOLUTION FUNCTIONS

The numerical solution is obtained by application of the principle of stationary potential energy (ref. 6), using the functional  $I(y_\alpha, \lambda)$  in which  $\lambda$  is an unknown constant. The solution functions  $y_\alpha$  are taken as two-dimensional finite series

$$y_1(r, \theta) = x_1(r, \theta) + \sum_{i=1}^M \sum_{j=1}^N a_{ij} y_1^{ij}(r, \theta)$$

$$y_2(r, \theta) = x_2(r, \theta) + \sum_{i=1}^M \sum_{j=1}^N b_{ij} y_2^{ij}(r, \theta)$$

where  $a_{ij}$  and  $b_{ij}$  are unknown coefficients. The symmetry and geometric boundary conditions evident in figure 11 are met by

$$y_1^{ij}(r, \theta) = r^i \sin(2j\theta)$$

$$y_2^{ij}(r, \theta) = r^i \sin[(2j-1)\theta]$$

The above functions allow the energy density to be integrated, thereby reducing the functional  $I$  to an algebraic function of the  $2 \times M \times N + 1$  unknown constants  $a_{ij}$ ,  $b_{ij}$ , and  $\lambda$

$$I = I(a_{ij}; b_{ij}; \lambda)$$

The functional  $I$  is made stationary by the constants obtained from the following set of simultaneous nonlinear equations:

$$\frac{\partial I}{\partial a_{ij}} = 0 \quad \text{and} \quad \frac{\partial I}{\partial b_{ij}} = 0 \quad \text{for } i = 1, 2, \dots, M \quad \text{and } j = 1, 2, \dots, N$$

$$\frac{\partial I}{\partial \lambda} = y_2(R, \pi/2) - R_\ell = 0$$

This system is solved in an iterative manner by the Newton-Raphson method. Using the starting values  $a_{ij} = b_{ij} = \lambda = 0$ , five or six iterations (which give successive corrections to these constants) are usually sufficient. The iterations are continued until the corrections appear to have negligible effect on the solution functions  $y_\alpha(r, \theta)$ . The energy density is evaluated after each iteration to check for minimization.

## DEFORMATION SOLUTION

Numerical results have been obtained using material constants  $\mu = 75$  psi (shear modulus),  $K = 475,000$  psi (bulk modulus), and  $k = 13.3$  in the Blatz-Ko model. The values of  $K$  and  $k$  are taken from reference 7 where they are shown to give a good fit to hydrostatic compression data on Butyl tread rubber (polyisobutylene). The shear modulus is believed to be a realistic estimate, based on Treloar's statement (ref. 9) that the shear modulus of rubber is lower than the bulk modulus by a factor of about  $10^4$ .

The computer-generated drawing below shows coordinate circles and radii before deformation ( $x_1$  and  $x_2$ , dashed lines) and the deformed configuration ( $y_1$  and  $y_2$ , solid lines) of these circles and radii. The deformation is produced by a 10-percent deflection of the contacting surface (shown dashed). The deformation solution,  $y_1(r, \theta)$  and  $y_2(r, \theta)$ , is obtained in a 16-term series for each function; the strain energy is minimized by the coefficients  $a_{ij}$  and  $b_{ij}$  for  $i=1,2,3,4$  and  $j=1,2,3,4$ , found after six Newton-Raphson iterations.

This computation took 30 seconds of CPU time on a mainframe computer (Amdahl 470/V8). The Lagrange multiplier obtained in this solution is  $\lambda=93.1$ , interpreted as a 93.1 lb load needed for a 10-percent deflection if the semicylinder extends 1 inch in the  $z$ -direction. (Fig. 14).

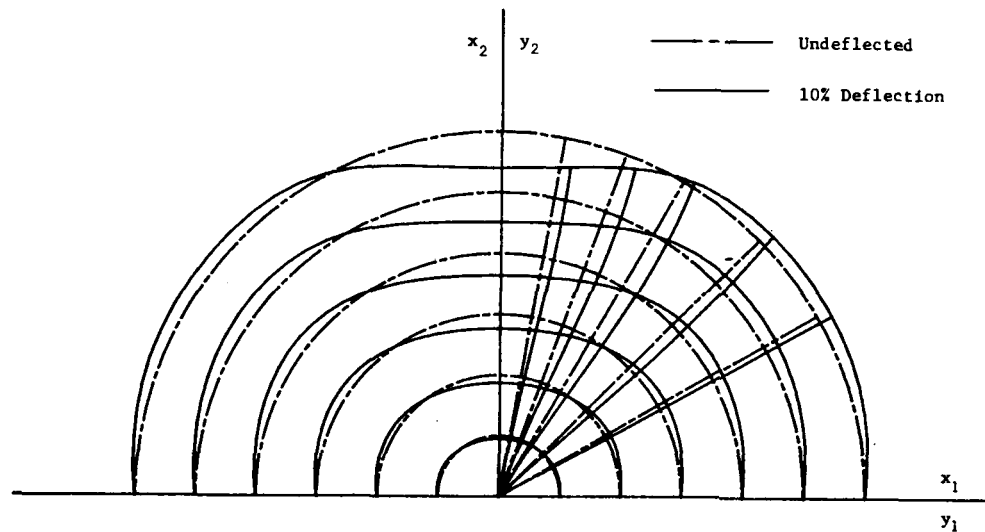


Figure 14

### III. STATIC AND ROLLING CONTACT FRICTION

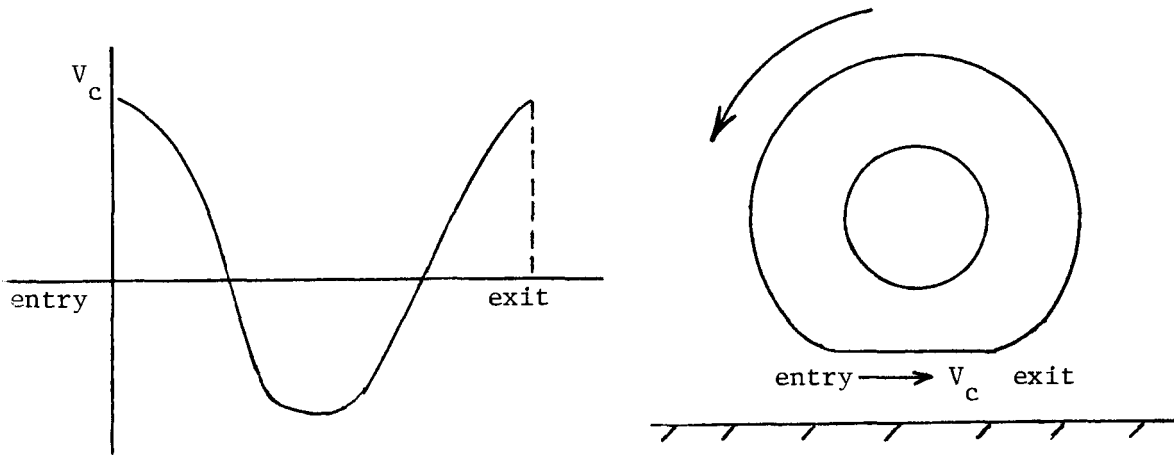
*Static Contact Friction.* A body is brought into static contact by motion perpendicular to the contact plane. During this motion, the contact boundary expands until the resultant of the normal contact pressure reaches equilibrium with the external load applied to the body. As the contact region is formed, shear forces are generated by tangential motion of contacting surface points. These shear forces are frictional and transient, reaching equilibrium levels when the body itself comes into equilibrium. Although the body may be assumed elastic, and thus conservative, the frictional shear forces are not conservative.

The formidable problem of calculating a static contact solution including the effect of friction is alleviated somewhat by assuming Coulomb's law of friction is valid in the contact region. An algorithm for including Coulomb friction in a static contact problem has been developed by Rothert et al. (ref. 10). Although Coulomb friction may be taken for an approximate analysis of frictional contact, mathematical and physical uncertainties arise when it is assumed. Nonclassical friction laws have been proposed by Oden and his coworkers (e.g., ref. 11). Although these appear to have been developed mainly for metals, they may be applicable to more deformable material such as rubber.

*Rolling Contact Friction.* This discussion is limited to steady rolling under a constant load. Neglecting hysteretic effects in the body, the power input to maintain steady rolling is balanced by the work rate of the friction forces in the contact region. In steady rolling, a contact region, whose boundary is fixed by the load, is continuously generated. The normal pressure and sliding velocity at a given location within the contact boundary do not change with time so steady-state frictional behavior is maintained. The rolling contact problem with friction is therefore much easier to analyze and provides a mechanism for the study of nonclassical friction theories. An algorithm for calculating friction in the contact region of a tire rolling at constant velocity will be described next.

## SLIDING TREAD MODEL

This is a tread element model developed to convert a frictionless rolling contact solution into a solution for rolling contact with friction. The element passes through the contact region with the velocity found for frictionless contact. This is termed the carcass velocity,  $V_c$ , whose distribution is symmetric about the center of the footprint as sketched below



For a free-rolling tire, the amplitude of the footprint sliding velocity is very small. At 60 mph (1056 ips), the peak  $V_c$  is calculated (by the author) to be about 50 ips in a frictionless footprint.

In free-rolling, the normal contact pressure distribution,  $p$ , is essentially unchanged by friction. The sliding velocity distribution, however, is significantly altered in an interactive manner. A hysteretic theory of tire-pavement friction proposed by Schapery (ref. 12) gives the dependence of the friction force,  $F_s$ , on the actual sliding velocity,  $V_s$ , and normal pressure,  $p$ , at a point in the contact region. This is expressed as

$$F_s = -B \operatorname{sgn}(V_s) |V_s|^a \times p^b \quad (\text{hysteretic theory})$$

where  $a$ ,  $b$ , and  $B$  are material friction properties. The sliding tread element model, shown in figure 15(a), is viscoelastic with stiffness and damping parameters  $K$  and  $c$ . Sliding friction,  $F_s$ , causes the element to deform, thereby influencing the sliding velocity  $V_s$ . The following nonlinear differential equation is integrated to calculate  $V_s$ .

$$\frac{dV_s}{dt} = \frac{K(V_c - V_s) + c\dot{V}_c}{c + \frac{dF_s}{dV_s}}$$

In this equation,  $dF_s/dV_s$  is the rate of change of sliding friction with sliding velocity. This can be obtained by differentiating the hysteretic theory given above or measured experimentally. Footprint transit time,  $t$ , is taken as the independent variable. The time is equivalent to location in the footprint for steady rolling.

Figure 15(b) shows a schematic diagram of the sliding tread model and its function in converting a frictionless sliding velocity distribution into sliding velocity influenced by friction.

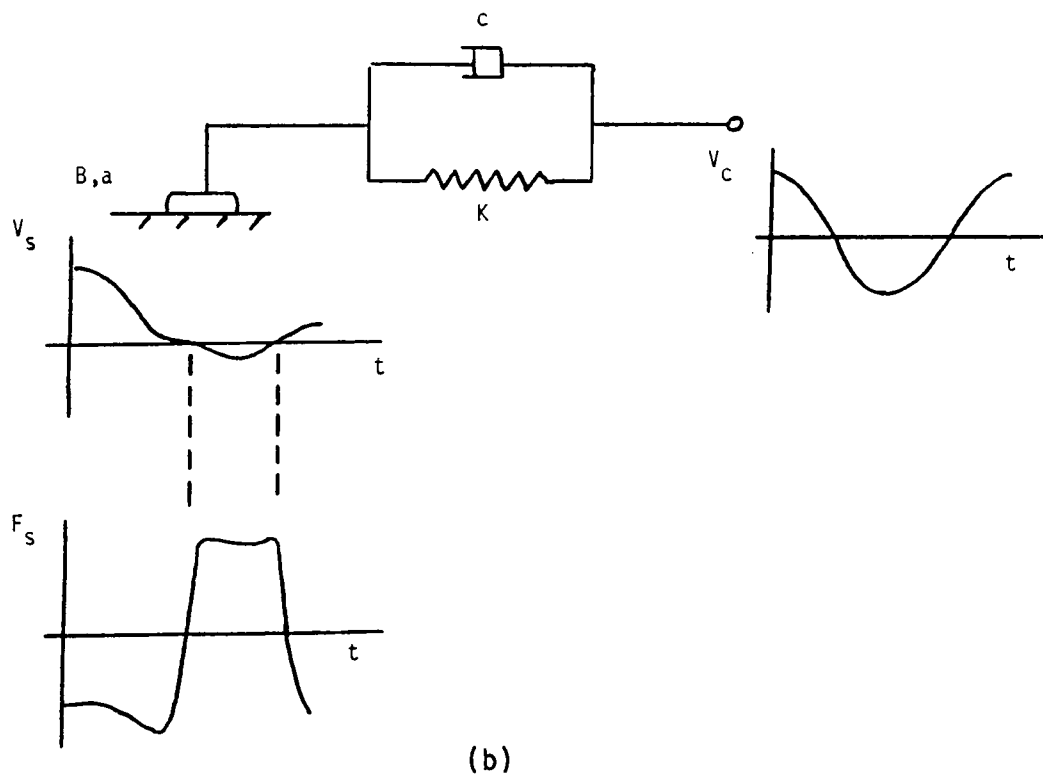
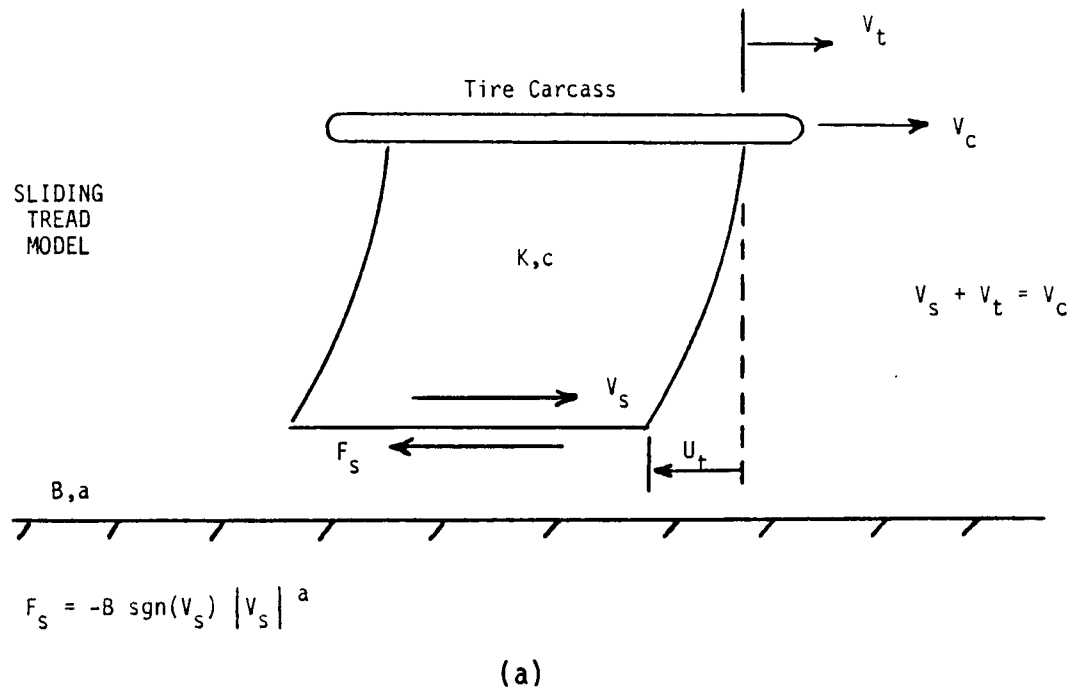


Figure 15

#### IV. FUTURE DIRECTIONS FOR CONTACT SOLUTION ALGORITHMS

As in other areas of solid mechanics, future research on contact problems will be directed towards obtaining solutions valid for large deformations. The finite-element method seems particularly well suited for application to contact problems and special elements have already been developed for this purpose. Continuum mechanics research on contact problems should not be neglected, however. A large-deformation contact solution in terms of continuous functions will prove valuable in the analysis of contact with friction and the assessment of friction laws now being proposed for deformable bodies.

A true contact problem is one in which the contact boundary and interfacial pressure distributions are unknown *a priori*. At present, it appears that such problems will be displacement prescribed: Deflection of the body toward the contact surface is specified and integration of the calculated normal component of the contact pressure gives the resultant load. Some effort should be directed towards a load-specified contact problem, perhaps utilizing the principle of stationary complementary energy to calculate the interfacial pressure distribution subject to the prescribed load constraint. Validated solutions for frictionless contact are essential prior to including the effect of friction on the contact solution.

In the analysis of friction, it seems that the study of rolling contact as a steady-state problem has much to offer. As friction is an interactive phenomenon, at least in regard to sliding velocity, sophisticated algorithms are needed to generate the frictional contact solution from the solution for frictionless contact (which will undoubtably be the starting point).

The following schematic, figure 16, outlines a progression of research on contact problems. Linear sliding contact is excluded from the outline as this is usually a transient situation leading to accelerated wear and abrasion. Much more will be gained by research focused on rolling contact which will, in any case, include sliding.

PROGRESSION OF RESEARCH ON FRICTIONAL CONTACT PROBLEMS

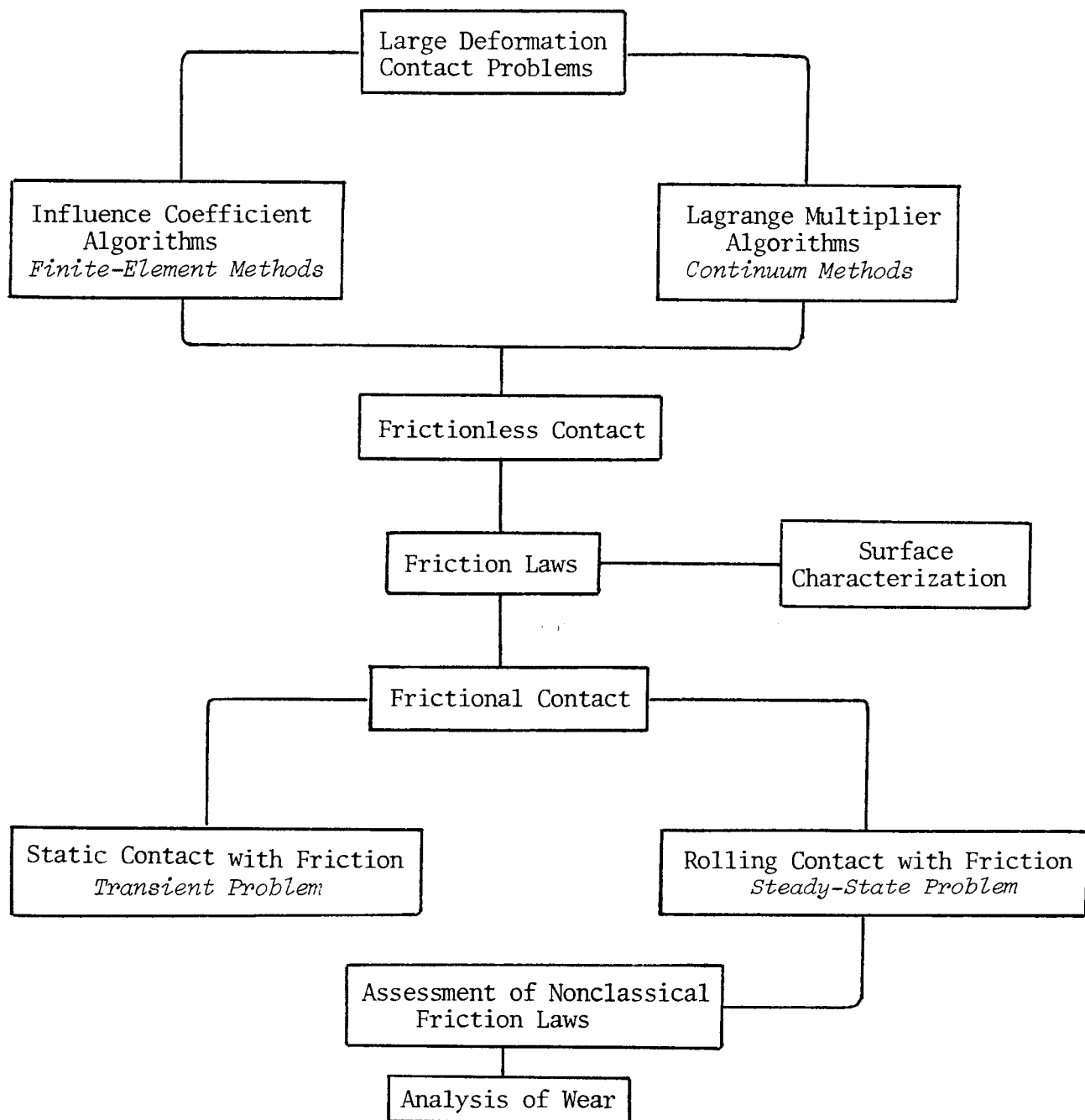


Figure 16

## REFERENCES

1. Tillerson, J.R.: and Haisler, W.E.: SAMMSOR II - A Finite Element Program to Determine Stiffness and Mass Matrices of Shells of Revolution. TEES-RPT-70-18, Texas A&M University, Oct. 1970.
2. Haisler, W.E.; and Stricklin, J.A.: SNASOR II - A Finite Element Program for the Statis Nonlinear Analysis of Shells of Revolution. TEES-RPT-70-20, Texas A&M University, Oct. 1970.
3. Schapery, R.A.; and Tielking, J.T.: Investigation of Tire-Pavement Interaction During Maneuvering: Theory and Results. Report No. FHWA-RD-78-72, Federal Highway Administration, June 1977.
4. Tielking, J.T.; and Schapery, R.A.: A Method for Shell Contact Analysis. Computer Methods in Applied Mechanics and Engineering, Vol. 26, No. 2, pp. 181-195, May 1981.
5. Green, A.E.; and Adkins, J.E.: Large Elastic Deformations. Oxford University Press, London, 1960.
6. Levinson, M.: The Application of the Principle of Stationary Potential Energy to Some Problems in Finite Elasticity. Journal of Applied Mechanics, Vol. 32, No. 3, 1965, pp. 656-660.
7. Blatz, P.J.; and Ko, W.L.: Application of Finite Elastic Theory to the Deformation of Rubbery Materials. Transactions of the Society of Rheology, Vol. 6, 1962, pp. 223-261.
8. Beveridge, G.S-G.; and Schechter, R.S.: Optimization: Theory and Practice. McGraw-Hill, 1970, p. 264.
9. Treloar, L.R.G.: The Physics of Rubber Elasticity, 2nd edition. Oxford University Press, London, 1958, p. 74.
10. Rothert, H.; Idelberger, H.; Jacobi, W.; and Niemann, L.: On Geometrically Nonlinear Contact Problems with Friction. Computer Methods in Applied Mechanics and Engineering, Vol. 51, 1985, pp. 139-155.
11. Oden, J.T.; and Pires, E.B.: Nonlocal and Nonlinear Friction Laws and Variational Principles for Contact Problems in Elasticity. Journal of Applied Mechanics, Vol. 50, No. 1, March 1983, pp. 67-76.
12. Schapery, R.A.: Analytical Models for the Deformation and Adhesion Components of Rubber Friction. Tire Science and Technology, Vol. 6, No. 1, February 1978, pp. 3-47.